

# Multi-color LUCAS: Lensfree On-chip Cytometry Using Tunable Monochromatic Illumination and Digital Noise Reduction

SUNGKYU SEO,<sup>1</sup> TING-WEI SU,<sup>1</sup> ANTHONY ERLINGER,<sup>1</sup> and AYDOGAN OZCAN<sup>1,2,3</sup>

<sup>1</sup>Electrical Engineering Department, University of California, Los Angeles, CA 90095, USA; <sup>2</sup>Biomedical Engineering IDP, University of California, Los Angeles, CA 90095, USA; and <sup>3</sup>California Nano Systems Institute (CNSI), University of California, Los Angeles, CA 90095, USA

(Received 25 July 2008; accepted 8 August 2008; published online 27 August 2008)

**Abstract**—It has been recently demonstrated that rapid on-chip monitoring of a *homogenous* cell solution within an ultra-large field-of-field of  $\sim 10\text{ cm}^2$  is feasible by recording the classical diffraction pattern of each cell in parallel onto an opto-electronic sensor array under incoherent white light illumination. Here we present several major improvements over this previous approach. First, through experimental results, we illustrate that the use of narrowband short wavelength illumination (e.g., at  $\sim 300\text{ nm}$ ) significantly improves the digital signal-to-noise ratio of the cell diffraction signatures, which translates itself to a significant increase in the depth-of-field (e.g.,  $\sim 5\text{ mm}$ ) and hence the sample volume (e.g.,  $5\text{ mL}$ ) that can be imaged. Second, we also illustrate that by varying the illumination wavelength, the texture of the recorded cell signatures can be tuned to enable automated identification and characterization of a target cell type within a *heterogeneous* cell solution. Third, a hybrid imaging scheme that combines *two different wavelengths* is also demonstrated to improve the uniformity and signal-to-noise ratio of the recorded cell diffraction images. Finally, we demonstrate that a further improvement in image quality can be achieved by utilizing adaptive digital filtering. These noteworthy improvements are especially quite important to achieve more reliable performance for rapid detection and counting of a target cell type among many other cells present within a heterogeneous sample volume of e.g.,  $\sim 5\text{ mL}$ . This incoherent on-chip imaging platform may have a significant impact especially for medical diagnostic applications related to global health problems such as HIV monitoring.

**Keywords**—High-throughput cell counting, On-chip imaging, Lensfree imaging, Lensless imaging, LUCAS, Incoherent imaging, Medical diagnostics, Point-of-care applications, Global health problems, HIV monitoring, Digital noise reduction, Adaptive filtering.

## INTRODUCTION

Starting with the discovery of cells in the 17th century, optical microscopes played a crucial role in exploiting the nature. Over the past century, there has been an extensive progress, which greatly extended the capabilities of optical microscopy based diagnostic tools, especially towards cell counting and characterization. One particular exciting achievement in microscopy was the development of novel on-chip microscopes that merged advanced micro-machining tools with microfluidics and digital signal processing.<sup>2,5,7,17</sup> Despite all these progress, even today, highly-accurate and high-throughput methods for selecting out a target cell population from a heterogeneous cell solution are needed for many applications in bioengineering and medicine. Currently, in clinical settings, the cell counting and characterization measurements are mostly conducted using flow-cytometry which demands complex and costly sample preparation steps within a bulky system.<sup>1,3,8,9</sup> On the other extreme, many researchers in bio-medicine still use a rather simple and crude technique such as a hemocytometer, which uses an optical microscope to count a calibrated sub-volume of the cell solution. This approach is still labor intensive; however it is inexpensive compared to flow-cytometry and provides a less accurate but a much simpler solution to cell counting.

Recently, we illustrated a high-throughput on-chip imaging platform that can rapidly monitor  $> 50,000$  cells within a *homogenous* solution over a field-of-view (FOV) of  $\sim 10\text{ cm}^2$ .<sup>16</sup> We refer to this technique as Lensfree Ultra-wide-field Cell monitoring Array platform based on Shadow imaging (LUCAS). In this earlier work, we showed that using incoherent white light illumination, the LUCAS platform can record the classical diffraction pattern of all the cells of the homogenous solution within a FOV of  $\sim 10\text{ cm}^2$  onto an opto-electronic sensor array such as a CCD

---

Address correspondence to Aydogan Ozcan, Electrical Engineering Department, University of California, Los Angeles, CA 90095, USA. Electronic mail: ozcan@ucla.edu  
Sungkyu Seo and Ting-Wei Su—Equal contribution.

(charge-coupled device) chip without using any lenses. In this manuscript, we present several significant improvements over the previous approach. We not only present, for the first time, a detailed analysis of the performance of this high-throughput LUCAS platform by quantifying the effects of the illumination wavelength ( $\lambda$ ), substrate thickness ( $S$ ), and refractive index ( $n$ ) on the recorded digital cell signatures, but also we illustrate that the use of a narrowband short wavelength illumination (e.g.,  $\lambda \sim 300$  nm) significantly improves the digital signal-to-noise ratio of the cell diffraction signatures. This improved signal-to-noise ratio translates itself to a significant increase in the depth-of-field (DOF) and hence the sample volume that can be analyzed. We also illustrate that by varying  $\lambda$ , the texture (i.e., the 2D pattern) of the recorded cell signatures can be tuned to enable automated identification and characterization of a target cell type within a *heterogeneous* cell solution. Thus, the results of this manuscript also describe the first demonstration of high-throughput on chip characterization of a *heterogeneous* cell solution using spatially incoherent *tunable wavelength illumination*. When compared to our previous work<sup>16</sup> which could only analyze a homogeneous cell solution, this constitutes a significant advancement.

In this manuscript, we further show that a hybrid imaging method that digitally combines two different wavelengths (e.g., 300 and 950 nm) can notably improve the uniformity and signal-to-noise ratio of the LUCAS diffraction images. We refer to this improved cell characterization scheme as *multi-color LUCAS*. Finally we demonstrate that a further signal-to-noise ratio improvement in multi-color LUCAS images can be achieved by utilizing adaptive digital filtering. All of these noteworthy improvements in the diffraction signature of each cell type help us to achieve a much better performance for specific detection of a target cell type among many other cells present within a heterogeneous sample volume of e.g.,  $\sim 5$  mL. The presented multi-color LUCAS platform may have a significant impact especially in resource scarce settings for medical diagnostic applications related to global health problems.

## MATERIAL AND METHODS

### *Multi-color LUCAS Set-up*

Our novel multi-color LUCAS platform can rapidly image/monitor multiple layers of cells, within a volume of  $\sim 5$  mL all in parallel without the need for any lens, microscope-objective, or any mechanical scanning. In multi-color LUCAS the classical diffraction pattern (i.e., the shadow) of each individual cell within the entire sample volume is detected in less than one second using an opto-electronic sensor array that is

illuminated with a spatially incoherent tunable wavelength source (see Fig. 1a and Supplementary Fig. S1). The acquired shadow image is then digitally processed using a custom developed “decision algorithm” to enable both the identification of the cell location in 3D and the characterization of each cell type within the sample volume. The characteristic diffraction signature of each cell or micro-object type strongly depends on the refractive index, 3D morphology, and the height of the cell/micro-object from the sensor array surface, as well as the illumination wavelength. Therefore, in multi-color LUCAS, many different cell types or other micro-objects will yield a uniquely different signature (see Fig. 1) which forms the basis of high-throughput automated characterization of a heterogeneous cell solution over a FOV of  $\sim 10$  cm<sup>2</sup> and a DOF of  $\sim 5$  mm, corresponding to a total volume of  $\sim 5$  mL. As a proof-of-principle, Fig. 1b shows a single frame LUCAS image for 3T3 cells (fibroblasts) that is acquired in less than one second using the set-up of Fig. 1a over a FOV of  $\sim 10$  cm<sup>2</sup>. The insets of Fig. 1b also show the zoomed images of various points on the LUCAS image illustrating the unique diffraction signatures of individual 3T3 cells. This figure illustrates the fact that LUCAS can monitor a field of view that is  $\sim 2$  orders of magnitude wider than a regular light microscope, highlighting its high-throughput nature.

Since LUCAS is a lensless system, there is no optical magnification and the resolution of the recorded images is quite poor. This, however, is not a limitation for LUCAS since the diffraction patterns of different cells and other micro-objects exhibit uniquely different textures as discussed above; see e.g., Fig. 1, right bottom panel for the individual diffraction signature of a red blood cell (RBC), hepatocyte, fibroblast, mouse embryonic stem (mES) cell, and yeast cells (*S. Pombe*; fixed and alive). Note that even for the same cell type, e.g., alive vs. fixed yeast cells, the diffraction signatures are uniquely different. This feature of LUCAS enables automated counting and characterization of various different cells within a heterogeneous solution even with highly pixelated low resolution diffraction images. A further discussion on the details of this automated high-throughput cell characterization algorithm will be provided in the following sections.

## RESULTS AND DISCUSSION

### *Evolution of the Diffraction Signature in Multi-color LUCAS as a Function of the Depth of Field, Substrate Thickness, and Refractive Index*

One of the most important merits of the LUCAS platform is that it permits characterization and 3D

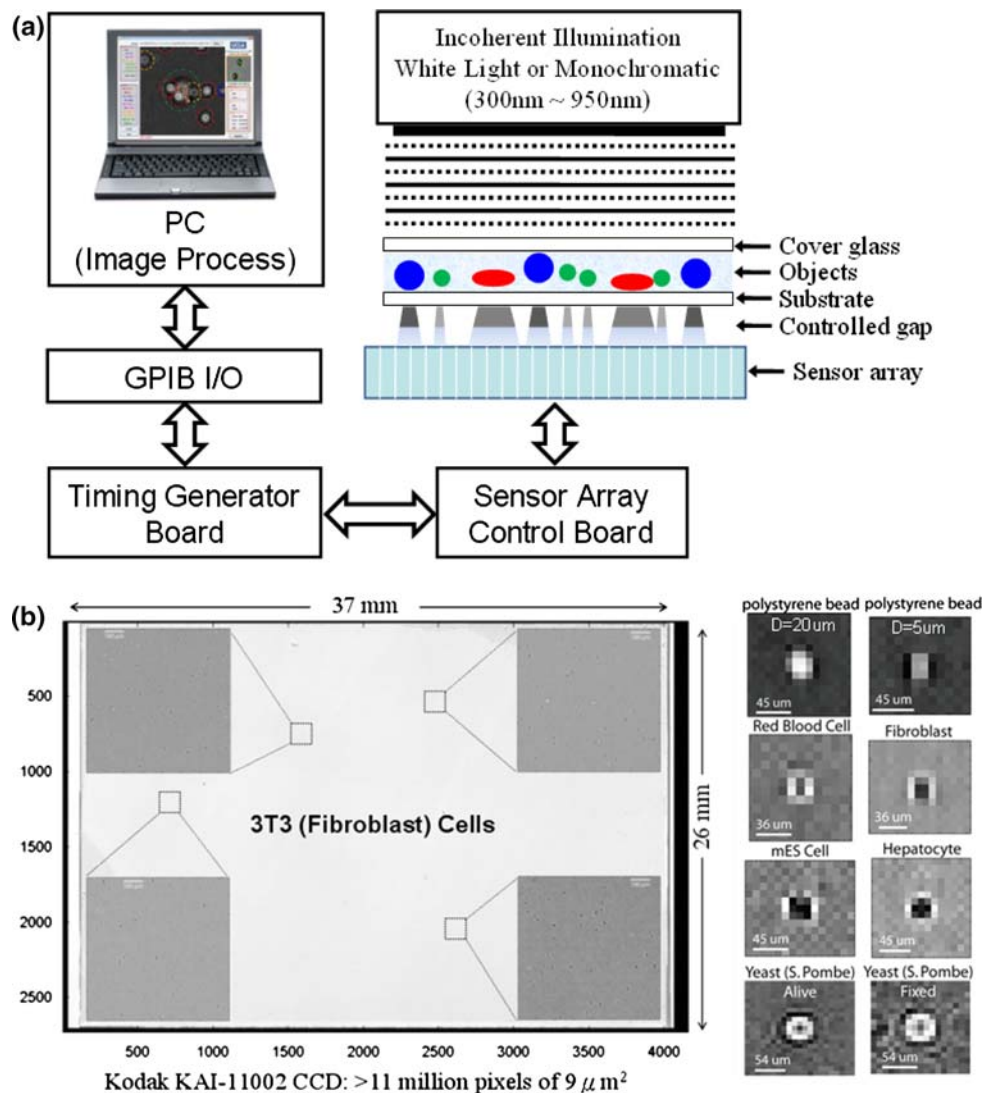


**FIGURE 1.** (a) Schematic diagram of the multi-color LUCAS platform. (b) Single frame LUCAS image for 3T3 (fibroblast) cells imaged using the set-up of (a). The insets of (b) show the zoomed images of various different points on the LUCAS image illustrating that the entire FOV of  $\sim 10$  cm<sup>2</sup> can be used for the identification and characterization of 3T3 cells. 8 Different images of the right bottom panel show the unique LUCAS signatures of polystyrene micro-beads ( $D = 20$  and  $5$  μm), red blood cell, fibroblast, mES, hepatocyte, yeast cell (S. Pombe; fixed and alive).

localization of different micro-objects within a much longer DOF than a regular wide-field microscope can achieve. To quantify the extended DOF of LUCAS and to better understand the properties of the LUCAS platform, we measured the evolution of the LUCAS diffraction pattern for various different sized micro-objects, as a function of the height ( $S$ ) of the particle from the sensor array plane. The results of these measurements are summarized in Fig. 2 for polystyrene micro-beads (2000 series, Duke Scientific) where the diameter of the particles were chosen to be  $D = 5, 10,$  and  $20$  μm. In this figure, we defined  $S/n = (S_{\text{glass}}/n_{\text{glass}} + S_{\text{air}}/n_{\text{air}})$ , where  $S_{\text{glass}}$  refers to the thicknesses

of the glass substrate and  $S_{\text{air}}$  refers to the thickness of the controlled air gap between the substrate and the sensor array.  $n_{\text{glass}} = 1.47$  and  $n_{\text{air}} = 1$  are refractive indices of glass and air, respectively.<sup>20</sup> Figure 2c illustrates the acquired LUCAS images of different sized micro-beads where  $S/n$  was varied between 68 and 3852 μm. To better quantify the changes in the recorded diffraction patterns, the digital signal-to-noise ratio (SNR) and shadow diameter (SD) were calculated for each image, where  $\text{SNR} = |(\max(I) - \mu_b)/\sigma_b|$ ,  $I$  is the light intensity on the sensor array, and  $\mu_b$  and  $\sigma_b$  are the mean and variance of background noise region. For shadow diameter calculations, we used the concept of

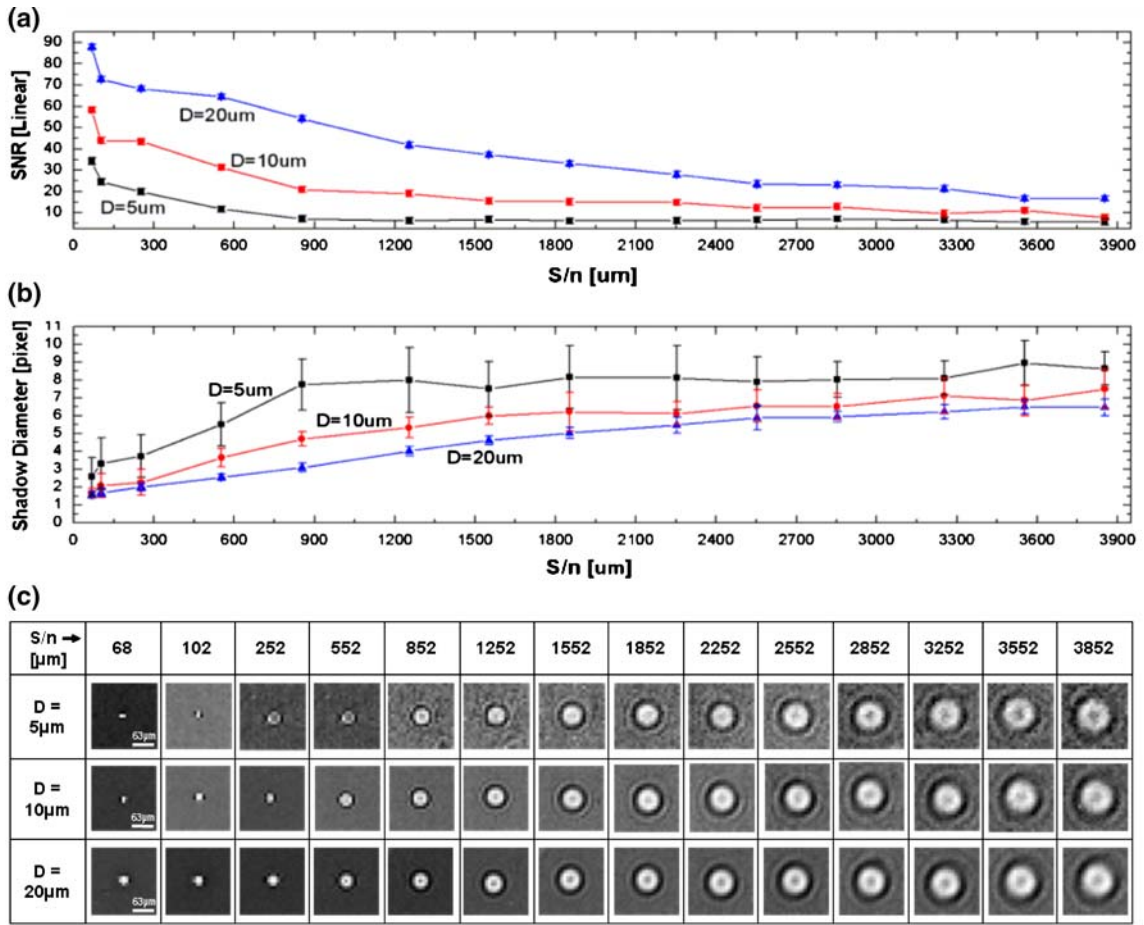


FIGURE 2. Evolution of the LUCAS diffraction signatures of polystyrene micro-beads at various different  $S/n$  values. (a) The variation of the image SNR as a function of  $S/n$  is illustrated for different bead sizes. Each data point was averaged from 20 different micro-beads in the same LUCAS image. (b) The variation of the shadow diameter (SD) as a function of  $S/n$  is illustrated. (c) The evolution of the LUCAS images of different sized microbeads is shown at different imaging conditions.

root-mean-square (RMS) width which was defined as  $SD = 2\sqrt{\frac{\sum_{x=1}^W (x - \bar{x})^2 |f(x)|^2}{\sum_{x=1}^W |f(x)|^2}}$ , where  $W$  is the maximum number of pixels in the region of interest, and  $\bar{x} = \left(\frac{\sum_{x=1}^W x |f(x)|^2}{\sum_{x=1}^W |f(x)|^2}\right)$ . In this formalism,  $x$  and  $f(x)$  denote the index of the image pixel and the detected signal intensity at each pixel, respectively.<sup>18</sup> Based on these definitions, Fig. 2a revealed that for all the measurements corresponding to different sized micro-objects, the SNR was higher for smaller  $S/n$  values. This result is expected since for small  $S/n$  values the diffraction based spreading of the shadow of each cell will be reduced increasing the optical SNR of the LUCAS image. As a result of this, small  $S/n$  values also necessitate smaller shadow diameters (SD) as verified in Fig. 2b. Another interesting observation is that as  $S/n$  becomes larger, although SNR drops rapidly (Fig. 2a), the uniformity of the recorded diffraction patterns (i.e., digital similarity between any two images of the same

cell-object type) increases, which is particularly important to improve the accuracy of the automated pattern recognition analysis of the LUCAS images. However, this improved signature uniformity of larger SD values has its own issue: it degrades the high-throughput nature of LUCAS by consuming more pixels per cell signature image. Thus, we can conclude that there exists a fundamental trade-off mechanism in LUCAS, which can be summarized as such:

- (1) Choosing a smaller  $S/n$  value (i.e., a small DOF from the sensor array) increases the SNR and reduces the SD, which then improves the throughput of the LUCAS platform. Meanwhile, a reduced SD implies a reduction in the information content (i.e., texture) of the cell diffraction image.
- (2) Choosing a larger  $S/n$  value (i.e., a long DOF from the sensor array) improves the uniformity of the acquired LUCAS signatures, together with an improvement in the content of the texture/pattern



information for each particle/cell image. However, these advantages also come with a reduction in the throughput of the system, since more pixels are now utilized for each cell image.

A good understanding of this trade-off mechanism among SNR, SD, throughput and uniformity is critical to find a sweet-spot for an  $S/n$  value that can optimize the counting and characterization of a specific cell type within a heterogeneous solution with the least possible error rate. However, when imaging a large sample volume (e.g.,  $>2$  mL), it is unavoidable to have both small and large  $S/n$  values within the same LUCAS image. And this necessitates the use of more sophisticated imaging schemes such as a hybrid approach involving a long and a short wavelength of narrow-band illumination. The proof-of-concept of such a hybrid approach will further be discussed in the following sections.

To demonstrate the feasibility of 3D localization and characterization of all the micro-objects within an ultra-large volume, using the multi-color LUCAS setup of Fig. 1a we simultaneously imaged two layers of a heterogeneous solution that contained  $5\ \mu\text{m}$  diameter micro-beads, red blood cells, and yeast cells (*S. Pombe*, alive), all suspended in  $1\times$  phosphate buffered saline (PBS) solution (see Supplementary Fig. S1a). In this experiment, the total volume, that was imaged using LUCAS within less than one second was  $>2.3$  mL. Supplementary Fig. S1c–d are zoomed-in images of Fig. S1b, taken within white dotted and dashed frames, where each shadow signature is circled with different colors uniquely identifying both the type and height of the cells/micro-objects from the sensor array surface. Note that even when the shadows from different layers overlap, as shown in Fig. S1d, the characteristic diffraction pattern of different micro-objects may still be clearly identified, demonstrating the high-throughput nature of the LUCAS platform. However, for opaque micro-objects such an overlap may cause irreparable loss of the diffraction signature of some of the particles resulting in a statistical counting error. Meanwhile, for a sensor array having an active area of  $\sim 10\ \text{cm}^2$  with  $>10,000,000$  pixels, such statistically overlap of micro-objects can only result in an error rate of  $<10\%$  for  $\leq 50,000$  cells.

#### *Evolution of the Diffraction Signature in Multi-color LUCAS as a Function of the Illumination Wavelength*

Another important aspect of the multi-color LUCAS platform is that by varying the illumination wavelength, the texture (i.e., the 2D pattern) of the recorded cell images can be tuned to improve the digital image quality for automated identification

and characterization of a target cell type within a heterogeneous cell solution. In multi-color LUCAS, using a shorter wavelength of narrowband illumination improves the SNR especially for longer DOF values, by reducing the effect of diffraction. However, as discussed earlier, when the diffraction pattern of the cells get narrower, the 2D texture information that can be used to recognize the cell type becomes less discriminative. Figure 3 illustrates this effect on three different micro-objects, i.e.,  $5\ \mu\text{m}$  diameter micro-beads, red blood cells, and yeast cells (alive, *S. Pombe*). In Fig. 3, for  $S/n = 68\text{--}102\ \mu\text{m}$ , all micro-objects, regardless of the illumination wavelength, reveal a strong shadow signature, with relatively high SNR values ( $>22\ \text{dB}$ ) where  $\text{SNR} = 20 \cdot \log_{10} |(\max(I) - \mu_b) / \sigma_b|$ . However, since the diffraction signature of each cell/micro-object occupies a small number of pixels on the sensor array, the 2D texture of the recorded LUCAS images does not provide a rich source of information towards automated characterization of the acquired image. Meanwhile, when  $S/n$  was increased to  $>1000\ \mu\text{m}$  (see Fig. 3), as expected, a shorter illumination wavelength gave a higher SNR (by e.g.,  $>5\ \text{dB}$ ), while a longer illumination wavelength gave more discriminative texture for each cell/micro-object image. Striking effects of the shorter illumination wavelengths were evident especially at much longer DOF values corresponding to e.g.,  $S/n > 4000\ \mu\text{m}$ : for instance the shadow images of  $5\ \mu\text{m}$  diameter beads were not visible at  $S/n = 4102\ \mu\text{m}$  under white light illumination or  $825\ \text{nm}$  illumination, whereas at  $\sim 300\ \text{nm}$  illumination the micro-beads located at  $S/n = 4102\ \mu\text{m}$  could be clearly distinguished with a characteristic diffraction signature as illustrated in Fig. 3. The same behavior was also observed for red blood cell and yeast cell images (see Fig. 3).

To further illustrate the effect of the illumination wavelength on LUCAS images we performed a series of additional experiments for  $3\ \mu\text{m}$  diameter beads, red blood cells, alive and fixed yeast cells (*S. Pombe*), the results of which are summarized in Fig. 4 and the Supplementary Fig. S2. In these figures, notice that for longer wavelength of illumination (e.g.,  $\lambda = 825\ \text{nm}$ ), as opposed to white light illumination, the classical diffraction fringes around the object are quite dominant (see e.g. Fig. 4b). Since the 2D texture and the oscillation period of these fringes are unique for each micro-object type as illustrated in Fig. 4, this phenomenon can conveniently be used to improve the accuracy of the automated counting/characterization results by helping discrimination of a target cell type against e.g., other microparticles or dust. For white light illumination condition, however, such diffraction oscillations are much weaker, i.e., washed out due to superposition of various different patterns originating

Microbeads ( $D = 5 \mu\text{m}$ )	$\lambda = 300\text{nm}$	$\lambda = 600\text{nm}$	$\lambda = 825\text{nm}$	White Light
$S/n = 102 \mu\text{m}$	SNR=36.409 	SNR=27.802 	SNR=31.206 	SNR=29.942 
$S/n = 1102 \mu\text{m}$	SNR=26.260 	SNR=12.785 	SNR=8.215 	SNR=19.897 
$S/n = 3102 \mu\text{m}$	SNR=17.126 	SNR=10.953 	SNR=6.624 	SNR=12.727 
$S/n = 4102 \mu\text{m}$	SNR=12.100 	SNR=10.388 		

RBCs	$\lambda = 300\text{nm}$	$\lambda = 600\text{nm}$	$\lambda = 825\text{nm}$	White Light
$S/n = 68 \mu\text{m}$	SNR=32.287 	SNR=23.272 	SNR=26.389 	SNR=28.040 
$S/n = 1068 \mu\text{m}$	SNR=22.333 	SNR=14.205 	SNR=12.474 	SNR=14.778 
$S/n = 2068 \mu\text{m}$	SNR=17.136 	SNR=12.340 	SNR=6.513 	SNR=11.384 
$S/n = 3068 \mu\text{m}$	SNR=14.959 	SNR=8.534 	SNR=5.778 	SNR=8.128 
$S/n = 4068 \mu\text{m}$	SNR=8.556 	SNR=7.911 	SNR=4.287 	SNR=6.377 

Yeasts ( <i>S. Pombe</i> , Alive)	$\lambda = 300\text{nm}$	$\lambda = 600\text{nm}$	$\lambda = 825\text{nm}$	White Light
$S/n = 68 \mu\text{m}$	SNR=28.895 	SNR=26.898 	SNR=22.845 	SNR=28.676 
$S/n = 1068 \mu\text{m}$	SNR=24.650 	SNR=16.480 	SNR=12.846 	SNR=22.357 
$S/n = 2068 \mu\text{m}$	SNR=15.868 	SNR=15.014 	SNR=9.617 	SNR=17.494 
$S/n = 3068 \mu\text{m}$	SNR=10.941 	SNR=9.619 	SNR=8.428 	SNR=13.727 
$S/n = 4068 \mu\text{m}$	SNR=7.606 	SNR=7.901 	SNR=7.162 	SNR=8.496 

FIGURE 3. The effect of the illumination wavelength on the LUCAS signature of micro-beads ( $D = 5 \mu\text{m}$ ), red blood cells, and yeasts (*S. Pombe*) is illustrated.

from multiple wavelengths contained within the white light spectrum. The fact that we observe these diffraction fringes in the LUCAS signatures even though our illumination is spatially incoherent suggests that, unlike holographic techniques, LUCAS simply records the classical diffraction pattern of the cells/micro-objects, where the scattered light from the particles interferes with itself, as opposed to interfering with a coherent reference (i.e., background) beam.

#### Automated Processing of Multi-color LUCAS Images

Being able to accurately and automatically count and analyze micro-objects within a large volume is of paramount importance to multi-color LUCAS platform. Towards this goal, we implemented an automated image processing program that uses a custom-developed “decision algorithm” that is specifically designed to analyze the raw diffraction images captured by the multi-color LUCAS platform. This decision algorithm identifies the type and the relative height of each cell/micro-object found within a heterogeneous cell solution. The decision algorithm uses a set of training LUCAS images corresponding to homogeneous populations to build a statistical image library for each cell/micro-object type at a given height. Once a statistical diffraction image library is formed by using e.g.  $> 50$  different shadow images of the same cell kind, various parameters and conditions can be set within the program before starting the counting/characterization process. Upon loading the LUCAS image of the heterogeneous cell mixture, the program automatically generates a histogram and scans the image for dust particles and unwanted objects, as well as for dead pixels by applying thresholding at various different levels. After these initial steps, we then specify what type of cells/micro-objects will be counted within the LUCAS image, defining which cell libraries need to be used. For reasons of accuracy, the cell counting algorithm is specifically designed to begin the counting process with the most distinguishable objects first. For a  $500 \times 500$  pixel image, the entire LUCAS analysis should only take a few seconds even with modest PC hardware specifications. Once the target micro-objects are automatically identified based on statistical training library images, their location are marked within the LUCAS image by colored pointers. The total count information of each micro-object type is also displayed in the graphical user interface in the bottom-left frame.

Our initial studies indicate that the accuracy of our decision algorithm varies based on the mixture of

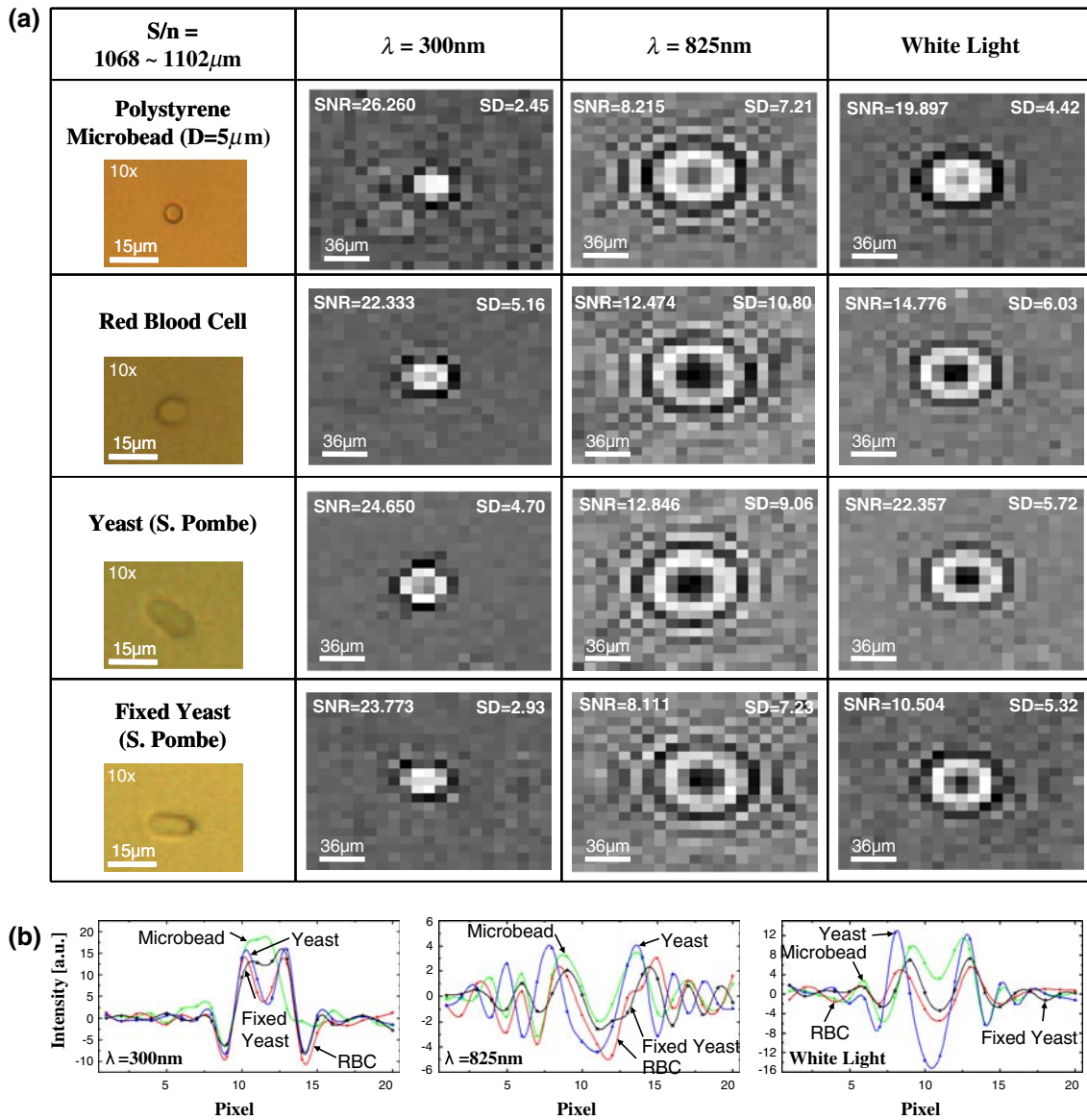


**FIGURE 4.** (a) Summary of the LUCAS diffraction signatures of polystyrene micro-beads ( $D = 5 \mu\text{m}$ ), red blood cells, and yeast cells (*S. Pombe*—alive and fixed) imaged under different illumination conditions is provided with quantitative comparison of SNR and SD values. (b) The cross-sectional profiles of the LUCAS signatures are illustrated, where each micro-object type shows unique differences in amplitude, oscillation period and functional behavior.

micro-objects to be analyzed in each sample. With homogenous mixtures containing only beads or red blood cells, a count accuracy as high as 98–100% was easily achieved. We also achieved a count accuracy of over ~90%, for artificial mixtures of e.g., red blood cells and hepatocytes imaged at a DOF of e.g.,  $< 500 \mu\text{m}$ . Meanwhile, for more complex heterogeneous solutions imaged at a longer DOF, such as a mixture of red blood cells, yeast cells and  $5 \mu\text{m}$  diameter micro-beads imaged at e.g.,  $S/n > 1000 \mu\text{m}$ , the raw LUCAS image can result in several sources of characterization errors due to reduced SNR and contrast as highlighted in Fig. 5a. In Fig. 5a, red triangles,

blue circles, and green squares mark the locations of RBCs, yeast cells, and micro-beads, respectively, which are automatically calculated using the decision algorithm applied to the raw LUCAS image of this heterogeneous mixture located at  $S/n = 1068 \mu\text{m}$ . In the same figure, we also marked the errors made in the calculated results with white triangles showing the error location and its type. A white triangle with the number “(1)” points to a cell/microbead that is “missed” by our decision algorithm; a white triangle with the number “(2)” points to a cell/microbead whose type identification is incorrect; and a white triangle with the number “(3)” points to an object that



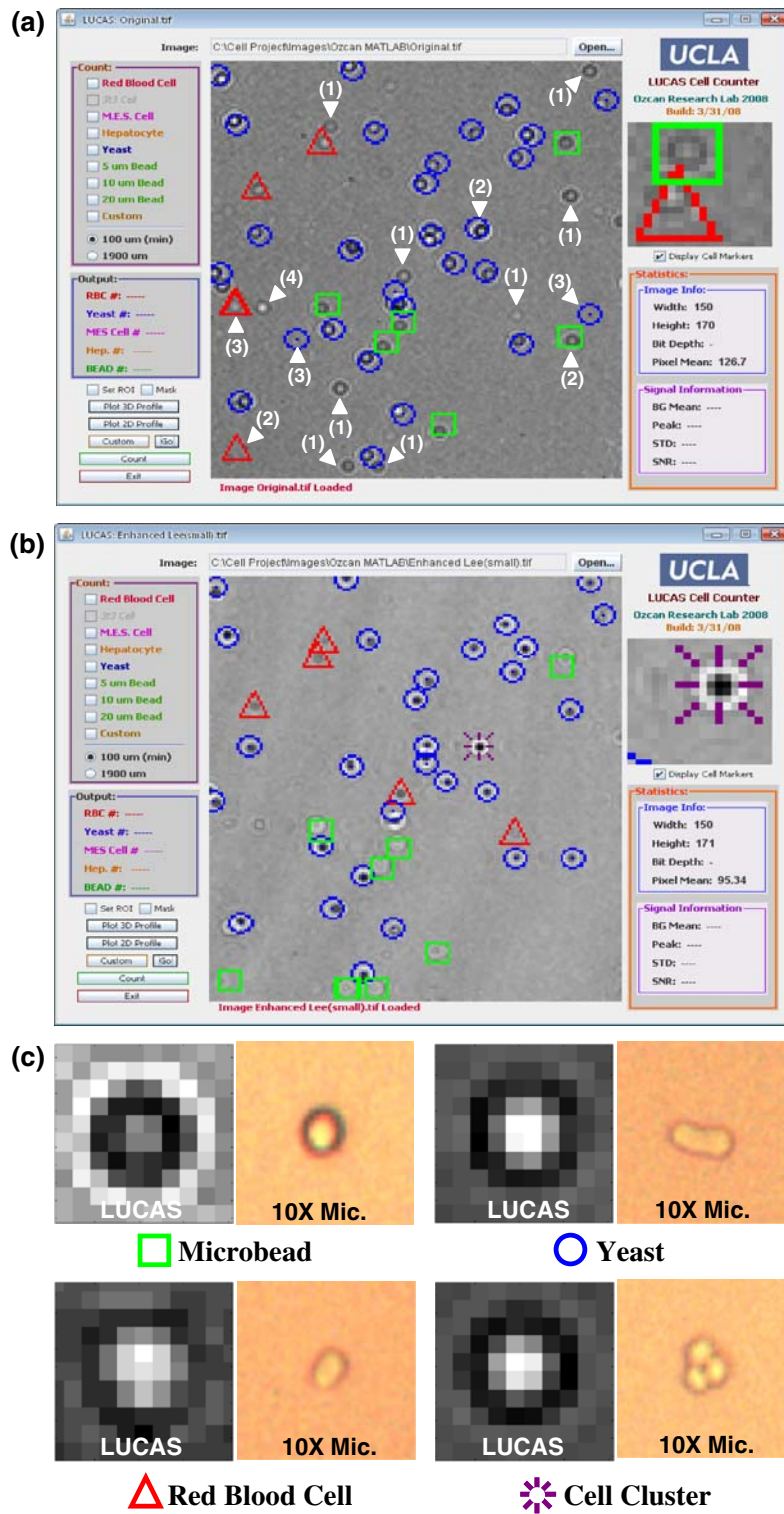
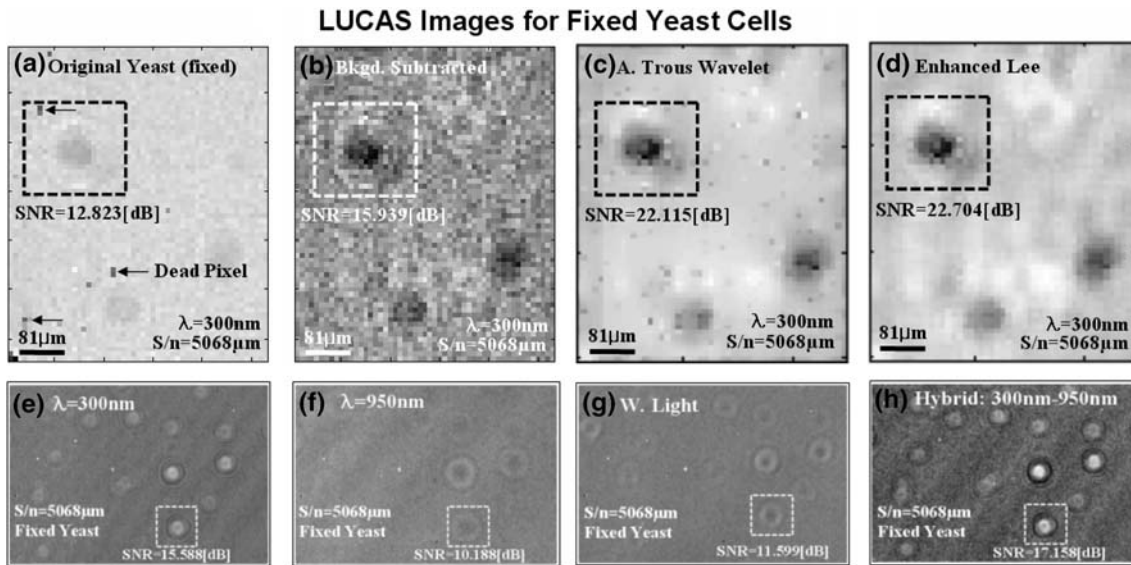


FIGURE 5. LUCAS automated characterization results for a heterogeneous solution imaged at  $S/n = 1068 \mu\text{m}$  and  $\lambda = 300 \text{ nm}$ . (a) Red triangles, blue circles, and green squares mark the locations of RBCs, yeast cells, and micro-beads, respectively, which are automatically calculated using the decision algorithm applied to the raw LUCAS image of this heterogeneous mixture. We also marked the errors made in the calculated results with white triangles showing the error location and its type (see text). (b) For the same region of interest, the same “decision algorithm” can yield a count/characterization accuracy of 100% by utilizing a digital filter (e.g., Enhanced Lee filter) that enhances the SNR and the image quality of the LUCAS signatures. (c) Zoomed LUCAS and 10× microscope images of the same micro-objects are shown.





**FIGURE 6.** (a–b) By implementing background image subtraction, dead pixels of the sensor array were successfully removed, resulting in an SNR improvement of 3.1 dB. (c–d) The improved performance of two different digital noise reduction filters, i.e., ‘A Troun Wavelet’ and ‘Enhanced Lee’ filters, is illustrated, enabling an SNR enhancement of 9.3 and 9.9 dB, respectively. (e–h) A hybrid LUCAS image that is obtained by subtracting the 300 nm LUCAS image from the 950 nm image provides a significant SNR enhancement as illustrated in (h), as well as effective elimination of the dead pixels of the sensor array.

should not have been counted (i.e., a false count). As shown in Fig. 5a, for this heterogeneous mixture, the processing of the raw LUCAS image at  $\lambda = 300$  nm yielded an error rate of  $\sim 15\text{--}60\%$  for different micro-objects. The main cause of this unacceptable performance is the reduced SNR and contrast of the LUCAS signature of each cell/microbead at long DOF values, where in this case  $S/n = 1068 \mu\text{m}$ .

However, as we illustrate in Fig. 5b for the same region of interest, our “decision algorithm” can yield a count/characterization accuracy of 100% by utilizing a noise reduction filter (e.g., Enhanced Lee filter) that digitally enhances the SNR and the image quality of the LUCAS signatures. As shown in Fig. 5b, the automated decision algorithm now corrects all of its errors made for the raw image (Fig. 5a) by using the digitally filtered LUCAS image. These results demonstrate the proof-of-principles of the developed decision algorithm to automatically analyze LUCAS diffraction images that are digitally processed/filtered to significantly improve the characterization accuracy. Starting next section we quantify in greater detail several approaches to enhance the SNR and the image quality of the acquired LUCAS signatures to significantly boost the characterization and counting performance of our custom-developed decision algorithm for heterogeneous cell solutions. A more detailed investigation of the statistical error rate of these different approaches will be provided in a future publication.

#### *Noise Reduction in Multi-color LUCAS Images*

As illustrated in the previous section, to improve the automated characterization accuracy of multi-color LUCAS images, digital noise reduction in the raw image can be effectively utilized. In LUCAS platform, there are several noise sources such as potential dust or unwanted micro-particles on the sensor surface or within the sample volume; dead pixels in the sensor array; or detector noise (e.g., relative intensity noise, read-out noise, etc.). All of these noise terms degrade the quality of the raw LUCAS image, which then translates itself to an increased error rate for automated cell counting results as highlighted in Fig. 5a. We implemented several image improvement methods, i.e., background image subtraction, use of multiple wavelengths, and use of digital noise reduction filters to minimize the effects of these noise artifacts on the performance of the multi-color LUCAS platform. Starting next section, we evaluate the success of each of these noise reduction approaches.

#### *Background Image Subtraction*

To improve the LUCAS image quality, we subtracted a background image of the sensor array without any object being present from the acquired LUCAS image. Such an approach is especially useful to remove the undesired effect of dead pixels on the sensor array. Figures 6a–6b show the improvement in

the LUCAS image that we achieved by using background subtraction for fixed yeast cells (*S. Pombe*) imaged at a DOF of  $\sim 5$  mm using a narrowband illumination wavelength of 300 nm. By implementing the background image subtraction, dead pixels (see arrows in Fig. 6a) of the sensor array were removed from the LUCAS image with an SNR improvement of  $>3$  dB.

#### *Use of Multiple Wavelengths: Hybrid LUCAS Images*

As discussed earlier, there is a trade-off among SNR, SD, throughput and uniformity of each LUCAS image. Using a shorter wavelength improves the SNR especially for longer DOF values by reducing the effect of diffraction. However, as discussed earlier, when the diffraction pattern of the cells gets narrower, not only the uniformity of the LUCAS signatures becomes an issue, but also the 2D texture information that can be used to recognize the cell type becomes less discriminative. To provide a solution to this trade-off, one possibility is to use a combination of a short and a long wavelength of illumination as illustrated in Figs. 6e–6h and Supplementary Fig. S3. Figures 6e–6g show the diffraction images of fixed yeast cells at a DOF of  $\sim 5$  mm for 300, 950 nm, and white light illumination, respectively. Meanwhile, Fig. 6h is a hybrid LUCAS image that is obtained by digitally subtracting the 300 nm image from the 950 nm one. With this hybrid LUCAS image, we achieved a significant SNR enhancement ( $\sim 6$  dB) when compared to e.g., white light illumination (see Fig. 6). Furthermore, this hybrid approach also improved the homogeneity and the texture of the diffraction signatures especially at lower DOF values. As illustrated in the Supplementary Fig. S3a, at a lower DOF of  $S/n = 272 \mu\text{m}$ , an illumination wavelength of 300 nm exhibits issues of: (i) poor signature uniformity; and (ii) poor 2D texture/pattern per diffraction image. However, as shown in Fig. S3b, a longer illumination wavelength of 950 nm exhibits much richer texture information for each cell, together with a much better LUCAS signature uniformity. By digitally combining 300 and 950 nm LUCAS images, the advantages of using both a short and a long illumination wavelength can be claimed as illustrated in Fig. 6h and Supplementary Fig. S3d, yielding a better SNR, better signature uniformity and texture information.

#### *Noise Reduction in Multi-color LUCAS Images Using Digital Filtering*

LUCAS images also suffer from random noise processes such as read-out noise, which limits the contrast and the SNR of the acquired diffraction signatures, making automated characterization of LUCAS images

difficult especially at longer DOF values. To de-noise digital images, a substantial amount of signal processing research resulted in the development of powerful digital filters for reducing the effect of various different sources of noise while preserving the edge sharpness and/or the texture of the target signal.<sup>4,6,10–15,19</sup> Here we evaluated the performance of several noise reduction digital filters (i.e., enhanced Lee filter, Lee filter, Kuan filter, Yu filter, ‘A Trous’ wavelet transform filter, hybrid median filter, symmetric nearest-neighbor filter, average filter, and adaptive Wiener filter) on multi-color LUCAS images corresponding to fixed yeast cells and red blood cells placed at a DOF of  $S/n \approx 5$  mm. Exemplary results of these different noise reduction filters are shown in Figs. 6c–6d, Figs. S4 and S5. These results indicate that the digital SNR of the diffraction signatures of the cells/microparticles can be enhanced by  $\sim 10$  dB when compared to raw LUCAS images, enabling a significant increase in the accuracy of the decision algorithm as also illustrated in Fig. 5b. Among these different digital filters, the enhanced Lee filter which works based on computing the local coefficient of variation as a measure of the image homogeneity was particularly successful in improving the SNR of the LUCAS signatures without a noticeable loss of textural information or edge sharpness (see Figs. 6c–6d, Figs. S4 and S5).

## CONCLUSIONS

We presented a detailed analysis of the performance of the multi-color LUCAS platform by quantifying the effects of the illumination wavelength, substrate thickness and refractive index on the recorded digital cell signatures. Through experimental results, we illustrated that the use of narrowband short wavelength illumination significantly improves the digital SNR of the LUCAS signatures, which translates itself to a significant increase in the DOF and hence the sample volume that can be characterized. We also illustrated that by varying the illumination wavelength, the 2D texture of the recorded cell signatures can be tuned to enable automated identification and characterization of a target cell type within a heterogeneous solution. A hybrid imaging scheme that digitally combines two different wavelengths is also demonstrated to improve the uniformity and the SNR of the LUCAS images. Finally, we demonstrated that a further improvement in image quality can be achieved by utilizing adaptive digital filtering. These improvements in the LUCAS signature of each cell type are especially important to achieve a better performance for specific counting of a target cell type within a heterogeneous solution. The presented on-chip imaging platform may

find an important application especially in global health related problems such as CD4 cell counting for HIV patients.

#### ELECTRONIC SUPPLEMENTARY MATERIAL

The online version of this article (doi:[10.1007/s12195-008-0018-6](https://doi.org/10.1007/s12195-008-0018-6)) contains supplementary material, which is available to authorized users.

#### REFERENCES

- <sup>1</sup>Burger, D. E., and R. J. Gershman. Acousto-optic laser-scanning cytometer. *Cytometry* 9:101–110, 1988.
- <sup>2</sup>Cui, X., L. P. Lee, X. Heng, W. Zhong, P. W. Sternberg, D. Psaltis, and C. Yang. Lensless high-resolution on-chip optofluidic microscopes for *Caenorhabditis elegans* and cell imaging. *PNAS* 105:10670, 2008.
- <sup>3</sup>Darzynkiewicz, Z., B. Elzbieta, X. Li, W. Gorczyca, and M. R. Melamed. Laser-scanning cytometry: a new instrumentation with many applications. *Exp. Cell Res.* 249:1–12, 1999.
- <sup>4</sup>Fraser, S. I., and A. R. Allen. A speckle reduction algorithm using the ‘a trous’ wavelet transform. In: Proceedings of the IASTED International Conference on Visualization, Imaging and Image Processing (ACTA 2001), pp. 313–318, 2001.
- <sup>5</sup>Garcia-Sucerquia, J., W. Xu, S. K. Jericho, M. H. Jericho, I. Tamblyn, and H. J. Kreuzer. Digital in-line holographic microscopy. *Appl. Optics* 45:836–850, 2006.
- <sup>6</sup>Harwood, D., M. Subbarao, H. Hakalahti, and L. Davis. A new class of edge-preserving smoothing filters. *Pattern Recognit. Lett.* 6:155–162, 1987.
- <sup>7</sup>Heng, X., D. Erickson, L. R. Baugh, Z. Yaqoob, P. W. Sternberg, D. Psaltis, and C. Yang. Optofluidic microscopy: a method for implementing high resolution optical microscope on a chip. *Lab Chip* 6:1274–1276, 2006.
- <sup>8</sup>Hulett, H. R., W. A. Bonner, R. G. Sweet, and L. A. Herzenberg. Development and application of a rapid cell sorter. *Clin. Chem.* 19:813–816, 1973.
- <sup>9</sup>Kamentsky, L. A., D. E. Burger, R. J. Gershman, L. D. Kametsky, and E. Luther. Slide-based laser scanning cytometry. *Acta Cytol.* 41:123–143, 1997.
- <sup>10</sup>Kuan, D. T., A. A. Sawchuk, T. C. Strand, and P. Chavel. Adaptive noise smoothing filter for images with signal-dependent noise. *IEEE Trans. Pattern Anal. Mach. Intell.* 7:165–177, 1985.
- <sup>11</sup>Lee, J. S. Speckle analysis and smoothing of synthetic aperture radar images. *Comput. Graph. Image Process.* 17:24–32, 1981.
- <sup>12</sup>Lim, S. J. Two-dimensional Signal and Image Processing. Englewood Cliffs: Prentice Hall, 1990.
- <sup>13</sup>Lopes, A., R. Touzi, and E. Nesby. Adaptive speckle filters and scene heterogeneity. *IEEE Trans. Geosci. Remote Sens.* 28:992–1000, 1990.
- <sup>14</sup>Nieminen, A., P. Heinonen, and Y. Neuvo. A new class of detail-preserving filters for image processing. *IEEE Trans. Pattern Anal. Mach. Intell.* 9:74–90, 1987.
- <sup>15</sup>Ozcan, A., A. Bilenca, A. E. Desjardin, B. E. Bouma, and G. J. Tearney. Speckle reduction in optical coherence tomography images using digital filtering. *J. Opt. Soc. Am. A* 24:1901–1910, 2007.
- <sup>16</sup>Ozcan, A., and U. Demirci. Ultra wide-field lens-free monitoring of cells on-chip. *Lab Chip* 8:98–106, 2008.
- <sup>17</sup>Psaltis, D., S. Quake, and C. Yang. Developing optofluidic technology through the fusion of microfluidics and optics. *Nature* 442:381, 2006.
- <sup>18</sup>Saleh, B. E. A., and M. C. Teich. Fundamentals of Photonics. Hoboken: Wiley-Interscience, 2007.
- <sup>19</sup>Starck, J. L., F. Murtagh, and A. Bijaoui. Image Processing and Data Analysis; the Multiscale Approach. Cambridge: Cambridge University Press, 1998.
- <sup>20</sup>Weber, M. J. Handbook of Optical Materials. 2nd ed. Boca Raton: CRC Press, 2003.